

An industrial application of thermal convection analysis

***H. Kanayama**

Department of Mathematical and Physical Sciences, Faculty of Science,
Japan Women's University,
2-8-1, Mejirodai, Bunkyo-ku, Tokyo 112-8681, Japan

*Corresponding author: kanayamah@fc.jwu.ac.jp

Abstract

A coupling analysis of thermal convection problems is performed in this work. By approximating the material derivative along the trajectory of fluid particle, the characteristic curve (CC) method can be considered. The most attractive advantage of this method is the symmetry of the linear system, which enables some classic symmetric linear iterative solvers, like the conjugate gradient (CG) method or the minimal residual method (MINRES), to be used to solve the interface problem of the domain decomposition system. Applications to industrial problems are demonstrated to show the effectiveness of our approach.

Keywords: The characteristic curve method, Symmetric linear solvers, Finite element method, Domain decomposition method, Vending machines

1 Introduction

It is well known that the Galerkin approach for Navier-Stokes equations faces the problem caused by the nonlinear convective term, which yields the difficulty to obtain a numerical solution, and that the difficulty even increases with the Reynolds number. A lot of researchers contributed to solve this; the stiffness matrix was generally non-symmetric and some product-type methods^[1] such as GPBi-CG, Bi-CGSTAB, Bi-CGSTAB2 were utilized as the iterative solver for non-symmetric linear systems, like ADV_sFlow 0.5, which was one of our previous works.^{[2]-[4]} In this research, based on the approximation of the material derivative along the trajectory of fluid particle, a characteristic curve (CC) method^{[5],[6]} is employed to approximate the material derivative terms. The method is natural from the viewpoint of the simulation of physical phenomena; it is also advantageous as it renders the matrix of the linear system symmetric. When solving the interface problem of the Schur complement system, which is generated by the domain decomposition method (DDM), the symmetry enables the conjugate gradient (CG) method or the minimal residual method (MINRES) to be employed instead of product-type iteration solvers. Despite the fact that there is no sufficient theoretical proof to assure this convergence currently, the CG or MINRES method does show good convergence even in cooperation with several kinds of preconditioners^[7] including the balancing domain decomposition (BDD) preconditioner^{[2],[5]} in this research.

For thermal convection problems, some research^[8] has been shown in references. A number of researches^{[9]-[12]} about the CC method were done in the case of a single processor. However, rare research is done on the implementation of this scheme in the domain decomposition system, in which better computation results can be expected as the computation capability is extended. The purpose of our work is to apply the CC method to the Navier-Stokes equations and the convection-diffusion equation, and to enable the coupling analysis of these two kinds of applications.

A new parallel coupling thermal convection solver^[6] has been developed. Based on a CC method, the scheme can provide solvability for non-stationary thermal convection problems. The new solver

can reduce memory consumption compared with solvers of product-types. The computation speed is also improved, as is expected. The reliability and accuracy of numerical results have successfully been validated by comparing with the exact solution.^[6] Comparisons of our numerical results with results of other recognized solvers or available benchmarks also convince us that the application of the characteristic curve method to thermal convection problems has been a success. Accompanied with several new features, the new solver is speedy and worthy to be expected. As one member of the ADVENTURE system (<http://adventure.sys.t.u-tokyo.ac.jp/>), it will be published as an updated version of ADV_sFlow on the homepage after the in-house testing.

Finally, some practical applications are demonstrated for a vending machine^[13]. Non-stationary thermal convection problems are solved to show the effectiveness of the above approach.

In recent years, energy conservation has become an important topic in Japan. One focus of current research is the use of numerical analysis techniques to control cooling and heating systems in vending machines to improve their efficiencies and reduce their electric power consumptions. In this study, we report results of analyses using the ADVENTURE_sFlow parallel solver to study problems of thermal convection in mechanical components inside a vending machine.

The rest of this paper is organized into several sections. In Section 2, formulations related to thermal convection problems are introduced; the characteristic curve method, as well as the related finite element scheme is also demonstrated in this section. Models and various settings including boundary settings are described in Section 3 and Section 4, respectively. Section 5 shows numerical results obtained by using various models and boundary settings. Conclusions that can be drawn from current results are presented in Section 6.

2 Formulations

2.1 The thermal convection problem

Let Ω be a three-dimensional polyhedral domain with the boundary $\partial\Omega$. Using the Boussinesq approximation to couple the Navier–Stokes equations to the convection–diffusion equation, the conservation equations of momentum and mass are as follows;

$$\begin{cases} \frac{\partial u}{\partial t} + (u \cdot \nabla)u - 2\nu\nabla \cdot D(u) + \nabla p = g\beta(T_r - T) & \text{in } \Omega \times (0, \bar{t}), \\ \nabla \cdot u = 0 & \text{in } \Omega \times (0, \bar{t}). \end{cases} \quad (1)$$

Also, the thermal convection equation is given as

$$\frac{\partial T}{\partial t} + u \cdot \nabla T - a\Delta T = S \quad \text{in } \Omega \times (0, \bar{t}). \quad (2)$$

In Eqs. (1) and (2), $u = (u_1, u_2, u_3)^T$ is the velocity [m/s]; t is time [s]; ν is the kinematic viscosity coefficient [m²/s]; p is the gauge pressure normalized by the density [m²/s²] (hereafter p is shortly called pressure); $g = (g_1, g_2, g_3)^T$ is the gravity [m/s²]; β is the thermal expansion coefficient [1/K]; T is the temperature [K]; a is the thermal diffusion coefficient [m²/s]; S is the source term [K/s]; and D_{ij} is the rate of strain tensor [1/s] defined by

$$D_{ij}(u) \equiv \frac{1}{2} \left(\frac{\partial u_i}{\partial x_j} + \frac{\partial u_j}{\partial x_i} \right) \quad i, j = 1, 2, 3.$$

Though initial and boundary settings are described in details for different problems in Section 4, they are here written as follows;

$$u = \hat{u} \quad \text{on } \Gamma_u \times (0, \bar{t}), \quad (3)$$

$$T = \hat{T} \quad \text{on } \Gamma_T \times (0, \bar{t}), \quad (4)$$

$$a \frac{\partial T}{\partial n} = 0 \quad \text{on } (\partial\Omega - \Gamma_T) \times (0, \bar{t}), \quad (5)$$

$$\sum_{j=1}^3 \sigma_{ij} n_j = 0 \quad \text{on } (\partial\Omega - \Gamma_u) \times (0, \bar{t}), \quad (6)$$

$$u = u^0, T = T^0 \quad \text{in } \Omega \text{ at } t = 0, \quad (7)$$

where $\sigma_{ij} = -p\delta_{ij} + 2\nu D_{ij}(u) \quad i, j = 1, 2, 3$

with the Kronecker delta δ_{ij} and n is the unit normal vector. \bar{t} is the total time [s]; u^0 is the initial velocity [m/s]; T^0 is the initial temperature [K]; \hat{u} is the boundary velocity [m/s]; and T is the boundary temperature [K]. Γ_u and Γ_T are the velocity specified boundary and the temperature specified boundary, respectively.

As the weak form, the following system is considered;

$$\left(\frac{\partial u}{\partial t}, v \right) + ((u \cdot \nabla)u, v) + (2\nu D(u), D(v)) - (p, \nabla \cdot v) = (g\beta(T_r - T), v) \quad \text{for } v \in V, \quad (8)$$

$$-(\nabla \cdot u, q) = 0 \quad \text{for } q \in Q, \quad (9)$$

$$\left(\frac{\partial T}{\partial t}, \theta \right) + (u \cdot \nabla T, \theta) + (a \nabla T, \nabla \theta) = (S, \theta) \quad \text{for } \theta \in \Theta. \quad (10)$$

Here, $L^2(\Omega)$ denotes the space of square summable functions in Ω and $H^1(\Omega)$ is the space of functions in $L^2(\Omega)$ with derivatives up to the first order.

$$V(g_1) \equiv \{v \in (H^1(\Omega))^3; v = g_1 \text{ on } \Gamma_u\}, V \equiv V(0), \quad (11)$$

$$Q \equiv \{q \in L^2(\Omega)\}, \quad (12)$$

$$\Theta(g_2) \equiv \{\theta \in H^1(\Omega); \theta = g_2 \text{ on } \Gamma_T\}, \Theta \equiv \Theta(0), \quad (13)$$

where (\cdot, \cdot) denotes the L^2 - inner product over Ω .

2.2 The characteristic curve method

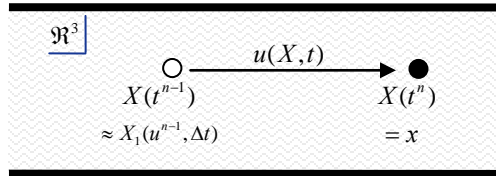


Figure1. Trajectory of a fluid particle

Let $X(t)$ be a function of position and Δt be the time increment. With the definitions of $t^n \equiv n\Delta t, N_T \equiv \lceil \bar{t}/\Delta t \rceil$, it is assumed that $X(t^n) = x$ and the fluid field velocity $u(X, t) = X'(t)$. A fluid particle's position at t^{n-1} can be approximated by

$$X(t^{n-1}) = X_1(u^{n-1}, \Delta t) + O(\Delta t^2), \quad (14)$$

where $X_1(u^{n-1}, \Delta t)(x) \equiv x - u^{n-1}(x)\Delta t$ is an approximation of the position function $X(t)$ ($t=t^{n-1}$) used by the Euler scheme^[12] (see Fig. 1). With this approximation, the material derivative term can be written as

$$\frac{\partial u}{\partial t} + (u \cdot \nabla)u = \frac{u^n - u^{n-1} \circ X_1(u^{n-1}, \Delta t)}{\Delta t}(x) + O(\Delta t). \quad (15)$$

Here, the notation \circ designates the composition of functions, u^n denotes the velocity at t^n , and u^{n-1} is a known value, which denotes the velocity at t^{n-1} .

2.3 Finite element scheme

Let Θ_h and $V_h \times Q_h$ be the piecewise linear finite element spaces for test functions of the convection-diffusion equation and Navier-Stokes equations, respectively, and \mathfrak{T}_h represents a triangulation (h is the diameter). With the following bilinear forms;

$$a_0(u, v) \equiv \int_{\Omega} 2\nu D(u) : D(v) dx, \quad b(v, q) \equiv - \int_{\Omega} q \nabla \cdot v dx, \quad (16)$$

the scheme for coupling analysis can be written as

for $n = 1, \dots, N_T, \forall \theta_h \in \Theta_h$ and $\forall (v_h, q_h) \in V_h \times Q_h$,

STEP 1: Find T_h^n by

$$\left(\frac{T_h^n - T_h^{n-1} \circ X_1(u_h^{n-1}, \Delta t)}{\Delta t}, \theta_h \right) + (a \nabla T_h^n, \nabla \theta_h) = (S, \theta_h). \quad (17.a)$$

STEP 2: Find (u_h^n, p_h^n) by

$$\begin{aligned} & \left(\frac{u_h^n - u_h^{n-1} \circ X_1(u_h^{n-1}, \Delta t)}{\Delta t}, v_h \right) + a_0(u_h^n, v_h) + b(v_h, p_h^n) + b(u_h^n, q_h) \\ & + \sum_{K \in \mathfrak{T}_h} \tau_K (\nabla p_h^n, -\nabla q_h)_K = (g \beta (T_r - T_h^n), v_h). \end{aligned} \quad (17.b)$$

Here, τ_K is a parameter of the stabilization term, which is used to smooth away the potential oscillation caused by P1/P1 elements. $(\cdot, \cdot)_K$ denotes the element wise inner product. In each non-stationary loop, STEP 1 and STEP 2 are performed. It keeps running until the maximum non-stationary loop number is reached.

3 Computational Models

In this study, we consider a simplified model for a vending machine depicted in from Fig. 2 to Fig. 4. Here, we have omitted the portions containing the cooling and heating systems and have retained only the columnar racks of canned beverages, the thermal barrier walls surrounding these racks, and the tilted ramp along which the cans slide inside the machine. The left panel of Fig. 2 depicts a side view of the model, while the right panel depicts a front view of the cross-sectional area indicated by the red line in the left panel. Below, we refer to components 1, 2, and 3 as x, y, and z, respectively.

The model used in the present analysis is a trapezoidal box with a height of 0.9 [m], a depth of 0.5676 [m], and a width of 0.1461 [m]. Air flows in from the slanted lower surface of the box and flows out through the upper surface. The cans that constitute the merchandise are 0.064 [m] in diameter and 0.114 [m] high. The separation between the cans and the thermal barrier walls is 0.01 [m] in the x direction. The cans and the intermediate board are separated from the thermal barrier walls by 0.014 [m] in the y direction. However, the number of cans depends on each model, and Fig. 2 and Fig. 4 are representative examples. Fig. 4(a), Fig. 4(b), and Fig.4(c) are models that have different number of cans.

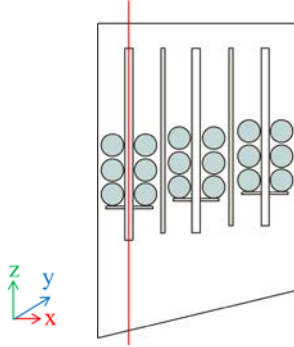


Figure 2. A side view of the model

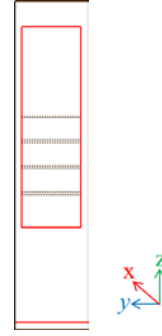


Figure 3. A front view of the model

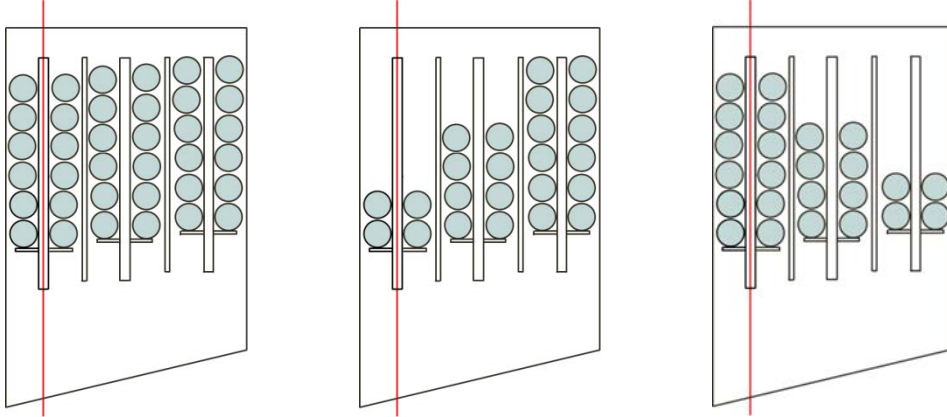


Figure 4. Side views of models which have different number of cans (a)full; (b)stairs; (c)stairs

4 Computational Conditions

4.1 Material properties

Table 1 lists the material properties used in the present analysis. In the winter case (Win.), an eddy viscosity constant is used for the first trial.

Table 1. Material properties

S [K/s]	ν [m ² /s]	T_r [K]	β [1/K]	a [m ² /s]
0	1.05×10 ⁻³ (Win.) 1.583×10 ⁻⁵ (Sum.)	300.15(Win.) 278.15(Sum.)	0.0034	2.207×10 ⁻⁵

4.2 Initial conditions and boundary conditions

The initial conditions are a uniform velocity of 0 [m/s] and a uniform temperature of 5[°C]. The boundary conditions have two types, which are Winter Condition 1 and Summer Condition 2. In Winter Condition 1, the airflow entry surface (the lower surface) is set as follows;

$$u_x = u_y = 0, u_z = 0.1 \text{ [m/s]},$$

$$T = 55 + 273.15 \text{ [K]}.$$

At the airflow exit,

$$\sum_{j=1}^3 \sigma_{ij} n_j = 0 \text{ [m}^2/\text{s}^2\text{]},$$

$$a \frac{\partial T}{\partial n} = 0 \text{ [m}\cdot\text{K/s]}.$$

At wall surfaces, the cans and the partitions within the machine,

$$u_x = u_y = u_z = 0 \text{ [m/s]},$$

$$a \frac{\partial T}{\partial n} = 0 \text{ [m}\cdot\text{K/s]}.$$

On the other hand, Summer Condition 2 are different from Winter Condition 1 in terms of temperature profile of entering air flow;

$$T = -2 \sim 4.5 \text{ [}^\circ\text{C]}.$$

In Summer Condition 2, we vary the temperature of the air flowing into the machine over the range -2 to 4.5 $^\circ\text{C}$. This is because, in actual vending machines, the cooling system is calibrated over time to reduce power consumption. The temperature profile used in this analysis is plotted in Fig. 5.

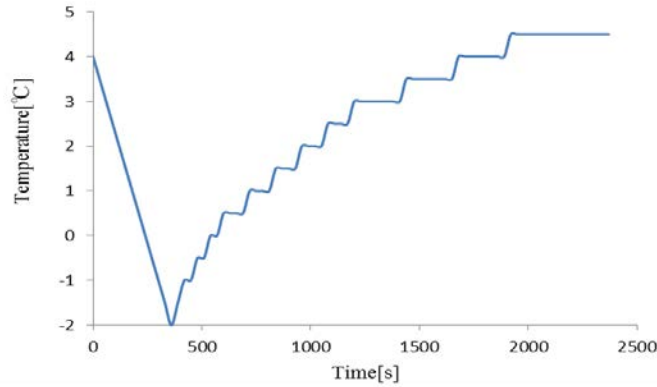


Figure 5. Temperature profile of entering airflow

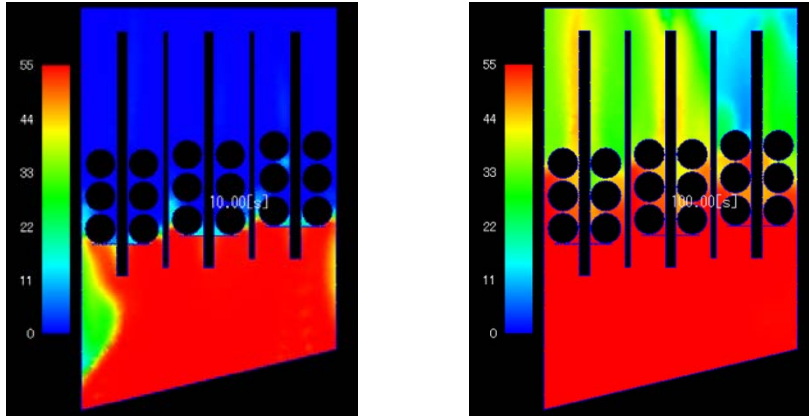
4.3 Other parameters

Numbers of elements, numbers of nodal points and degrees of freedom are 598,916, 148,757 and 743,785, respectively in the winter case. On the hand, they are, respectively, 744,585, 176,105 and 1,114,655 in the summer case. The time increment, numbers of time steps and the total time are 0.1 [s], 2,000 and 200 [s] in the winter case. They are, respectively, 0.1 [s], 24,000 and 2,400 [s] in the summer case. As the solver for (17.b), the CG method with the BDD preconditioner was used for the interface problem in the summer case, while the CG method with the Jacobi preconditioner was used for (17.a) and for (17.b) in the winter case. Using Core i7 920 (2.66 [GHz]) with 4 cores, it took about 5 hours by 5 PCs in the winter case and about 88 hours by 3 PCs in the summer case.

5 Results

5.1 Results of Winter Condition 1

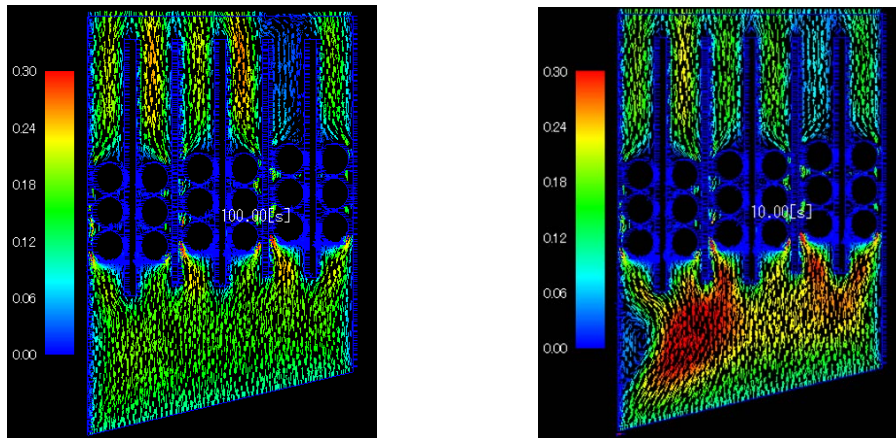
Figures 6(a) and 6(b) depict the temperature distributions after 10 and 100 [s] predicted by the model in Fig.2. Figures 7(a) and 7(b) plot the corresponding velocity vectors.



(a) after 10 [s];

(b) after 100 [s];

Figure 6. Temperature distribution



(a) after 10 [s];

(b) after 100 [s];

Figure 7. Velocity vectors

Figure 8 plots the temporal evolution of the temperature at the three points indicated in Fig. 8(a). Table 2 lists the coordinates of these three points.

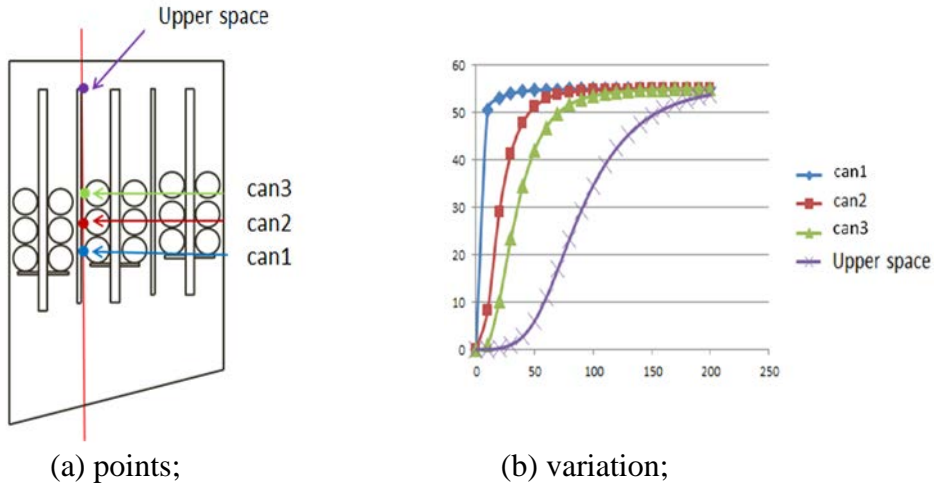


Figure 8. Temporal temperature variation

Table 2. Coordinates of points plotted in Figure 8

	$x[m]$	$y[m]$	$z[m]$
Can 1	0.1960	0.0738	0.4158
Can 2	0.1960	0.0738	0.4801
Can 3	0.1960	0.0738	0.5397
Upper space	0.1960	0.0738	0.8580

The computational results reveal that the temperature in the lower portion of the machine begins to rise first with the temperature in the upper portion of the machine gradually following. The flow achieves steady-state conditions at a surprisingly early time of 25 [s] because of the eddy viscosity constant, for which further study is required.

5.2 Results of Summer Condition 2

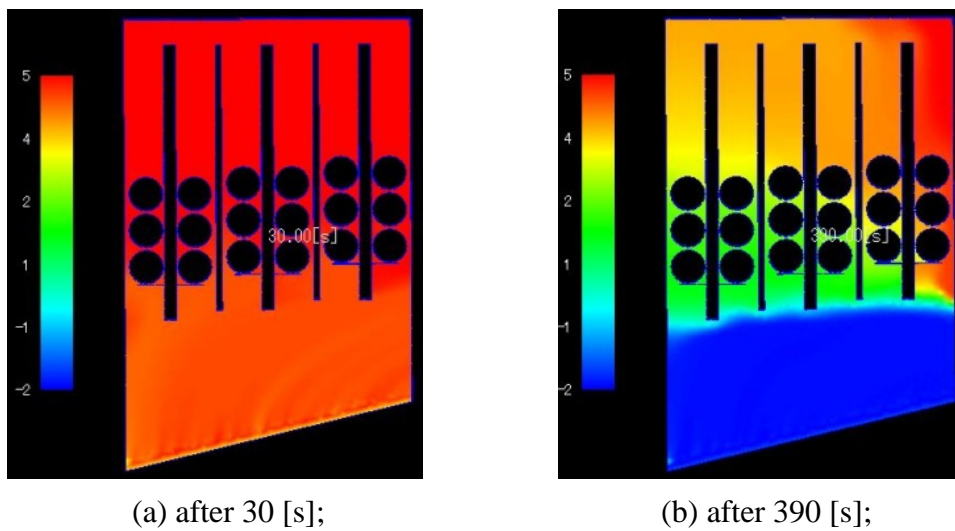
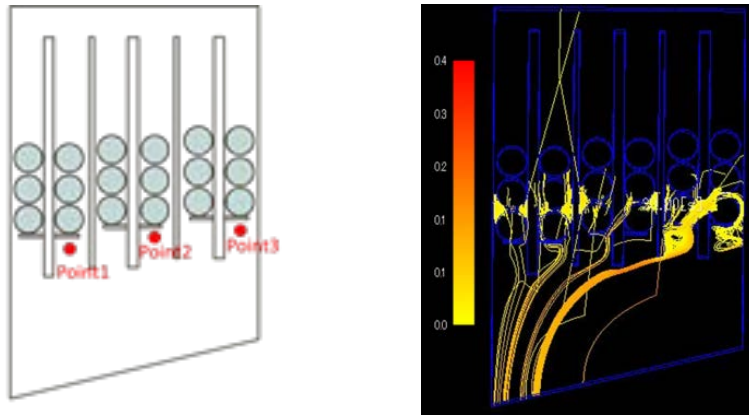


Figure 9. Temperature distribution

Table 3. Coordinates of three points for the temporal temperature variation

	x [m]	y [m]	z [m]
Point 1	0.136	0.073	0.321
Point 2	0.368	0.073	0.341
Point 3	0.524	0.073	0.361



(a) monitored;

(b) streamline diagram;

Figure 10. Three points for the temporal temperature variation

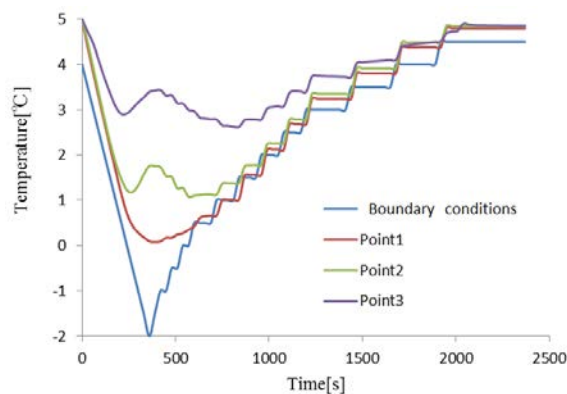


Figure 11. Temporal temperature variation at the three points depicted in Figure 10(a)

Figure 11 indicates that the temperature variation inside the vending machine follows that of the airflow into the machine. The airflow appears to be poor only in the region on the right side of the machine. To investigate this, we consider the streamline diagram of Fig. 10 (b), which indicates a counter flow along the surfaces of the cans in this region. The question of why such a counter flow arises entails many uncertainties and requires further study.

5.3 Summer case results of another models

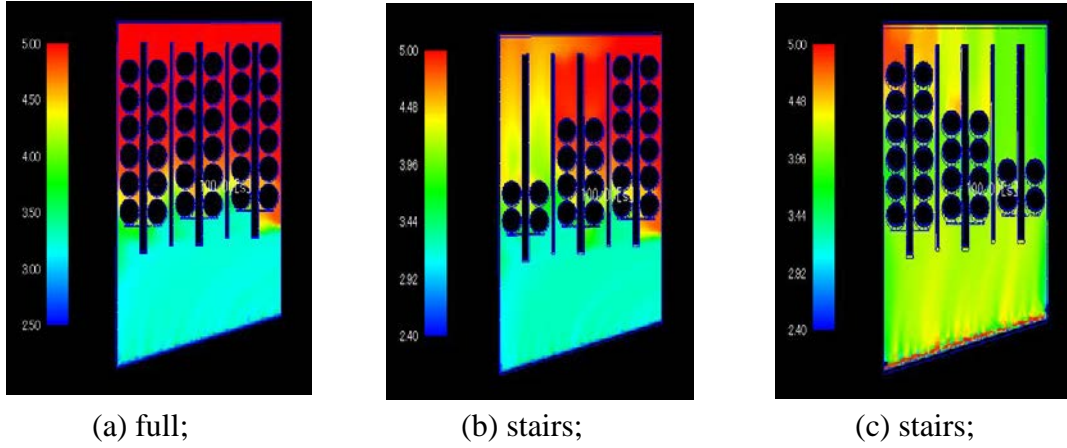


Figure 12. Temperature distribution after 100 [s]

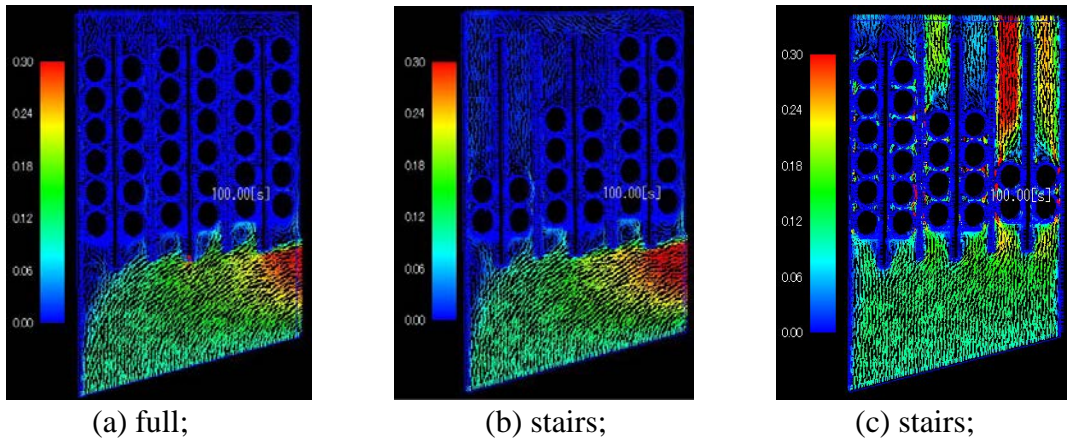


Figure 13. The temporal velocity variation of stream diagram after 100 [s]

Here, we consider another summer cases. Namely, different number of cans are considered for each column. Case (a) is a fully occupied case and Case (b) and Case (c) consider stairs. In all cases, many cans produce high temperature because cans become obstacles of the air flow. It is specially noted that Case (b) relatively shows high temperature, compared with Case (c).

6 Conclusions

A coupling analysis of thermal convection problems is performed in this work. By approximating the material derivative along the trajectory of fluid particle, the characteristic curve (CC) method can be considered. The most attractive advantage of this method is the symmetry of the linear system, which enables some classic symmetric linear iterative solvers, like the conjugate gradient (CG) method or the minimal residual method (MINRES), to be used to solve the interface problem of the domain decomposition system. Applications to industrial problems are demonstrated to show the effectiveness of our approach.

Acknowledgements

The first author would like to thank all support from Fuji Electric Co., Ltd. Also he gives sincere thanks to his past laboratory members in Kyushu University for their help. This work was supported by JSPS KAKENHI Grant Number 25840142.

References

- [1] Vorst, H.A. van der. Iterative Krylov method for large linear systems. Cambridge University Press, (2003).
- [2] Kanayama, H., Ogino, M., Takesue, N. and Mukaddes, A. M. M. Finite element analysis for stationary incompressible viscous flows using balancing domain decomposition. *Theoretical and Applied Mechanics* (2005) Vol. 54:211-219.
- [3] Kanayama, H., Komori, K., Sato D. and Sakuragi, O. Development of a thermal convection solver with hierarchical domain decomposition method. *Proceedings of Computational Engineering Conference of JSCEs* (2008) Vol. 13, No. 2: 721-722. (in Japanese)
- [4] Kanayama, H., Tsukikawa, H. and Ismail, I. Simulation of hydrogen dispersion by the domain decomposition method. *Japan Journal of Industrial and Applied Mathematics* (2011) Vol.28, No.1:43-53.
- [5] Yao, Q., Kanayama, H., Notsu, H. and Ogino, M. Balancing domain decomposition for non-stationary incompressible flow problems using a characteristic-curve method. *Journal of Computational Science and Technology* (2010) Vol. 4, No. 2:121-135.
- [6] Yao, Q. and Kanayama, H. A coupling analysis of thermal convection problems based on a characteristic curve method. *Theoretical and Applied Mechanics Japan* (2011) **59**:257-264.
- [7] Yao, Q., Kanayama, H., Notsu, H. and Ogino, M. Incomplete balancing domain decomposition for large scale 3-d non-stationary incompressible flow problems. *IOP Conference Series: Materials Science and Engineering* (2010) Vol. 10, No. 1: 012029.
- [8] Tabata, M. Finite element approximation to infinite Prandtl number Boussinesq equations with temperature dependent coefficients - thermal convection problems in a spherical shell. *Future Generation Computer Systems* (2006) Vol. 22:521-531.
- [9] Tabata, M. and Fujima, S. Robustness of a characteristic finite element scheme of second order in time increment. *Computational Fluid Dynamics 2004*(eds. Groth, C. and Zingg, D. W.) Springer-Verlag (2006):177-182.
- [10] Notsu, H. Numerical computations of cavity flow problems by a pressure stabilized characteristic-curve finite element scheme. *Transactions of the Japan Society for Computational Engineering and Science* (2008) Vol. 2008, No. 20080032, ONLINE ISSN : 1347-8826.
- [11] Notsu, H. and Tabata, M. A combined finite element scheme with a pressure stabilization and a characteristic-curve method for the Navier-Stokes equations. *Transactions of the Japan Society for Industrial and Applied Mathematics* (2008) Vol. 18, No. 3:427-445.
- [12] Pironneau, O. *Finite element methods for fluids*. John Wiley & Sons (1989).
- [13] <http://www.fujielectric.co.jp/frs/story/index.html>